Constraining Low-Energy Proton Capture on Beryllium-7 through Charge Radius Measurements

Emil Ryberg,[1] Christian Forssén,[1] H.-W. Hammer,[2,3] and Lucas Platter[4,1]

[1]*Department of Fundamental Physics, Chalmers University of Technology, 41296 Gothenburg, Sweden*

[2]*Institut für Kernphysik, Technische Universität Darmstadt, 64289 Darmstadt, Germany*

[3]*ExtreMe Matter Institute EMMI, GSI Helmholtzzentrum für Schwerionenforschung GmbH, 64291 Darmstadt, Germany*

[4]*Argonne National Laboratory, Physics Division, Argonne, IL 60439, USA*

(Dated: October 30, 2014)

Abstract

In this paper, we point out that a measurement of the charge radius of Boron-8 provides indirect access to the S-factor for radiative proton capture on Beryllium-7 at low energies. We use leading-order halo effective field theory to explore this correlation and we give a relation between the charge radius and the S-factor. Furthermore, we present important technical aspects relevant to the renormalization of pointlike P-wave interactions in the presence of a repulsive Coulomb interaction.

I. INTRODUCTION

A frequent problem encountered in nuclear astrophysics is that observables relevant to stellar and cosmological evolution cannot be measured directly in the laboratory. In many cases, this is due to the Coulomb barrier, which leads to very small cross sections at the low energies at which these processes occur in the stellar environment. Specifically, electroweak reactions relevant to big bang nucleosynthesis or solar astrophysics that involve either neutrinos or soft photons display this problem. A common strategy is then to carry out experiments of the desired observable at higher energies and to use models to extrapolate to the low-energy region. One process that has been analyzed frequently this way is radiative proton capture on ^{7}Be into ^{8}B. In the solar *pp* fusion reaction network, this reaction proceeds at $\sim$10 keV energies, and the subsequent beta decay determines the intensity of the high-energy part of the solar neutrino spectrum. The currently accepted threshold value of the corresponding S-factor

$$S(0) = (20.8 \pm 0.7(\text{expt.}) \pm 1.4(\text{theor.}))\ \text{eV b} \tag{1}$$

has been obtained by extrapolation of experimental data [1].

Effective field theory (EFT) provides an alternative way to obtain information on such observables. The EFT algorithm correlates a finite number of physical observables at each order, based on a power counting scheme that captures the relevant scales of the system. The simplest example might be the correlation between the scattering length a and the binding energy of two particles with mass m, $B_2 = 1/(ma^2)$, when a is positive and much larger than the range of the interaction R. The application of these ideas to nuclear physics has led to the development of the so-called pionless EFT, which is applicable for typical momenta below the pion mass. (See Refs. [2–4] for reviews and references to earlier work.) If one also introduces field operators for certain tightly bound clusters of nucleons, such as α particles, the pionless EFT is usually referred to as halo EFT [5, 6]. It has been applied to describe the structure and reactions of a number of known and suspected one- and two-neutron halo systems in the Helium [7, 8], Lithium [9–13], Beryllium [9, 10, 14], Carbon [9, 10, 15–17], and Calcium isotope chains [18].

For reactions with two or more charged particles, Coulomb effects are important. Although the Coulomb interaction is perturbative for intermediate and higher energies, it has to be treated nonperturbatively close to threshold. In the two-nucleon sector this was first

discussed by Kong and Ravndal for the proton–proton channel [19, 20] and later extended to next-to-next-to-leading order by Ando *et al.* [21]. A renormalization-group analysis of proton–proton scattering in a distorted-wave basis was performed in Refs. [22, 23] and $\alpha\alpha$ scattering, which is governed by a shallow S-wave resonance close to threshold, was discussed in Ref. [24]. The extension to describe the structure and charge radii of S-wave proton halo bound states with repulsive Coulomb interaction was recently carried out in Ref. [25].

Here we focus on ^{8}B as a loosely bound state of ^{7}Be-proton. This system has been considered previously in halo EFT by Zhang, Nollett and Phillips [26]. They calculated the S-factor of the reaction $^7\mathrm{Be}(p,\gamma)^8\mathrm{B}$ at leading order (LO) and obtained $S(0) = (18.2 \pm 1.2(\text{ANC only}))$ eV b consistent with the recommended value in Eq. (1). Moreover, they performed a detailed error analysis and investigated the sensitivity of their result to the input parameters. The scope of our work is somewhat different. Modern isotope shift measurements facilitate an extremely precise determination of the nuclear charge radius. We will show below that the charge radius of ^{8}B and the astrophysical S-factor of the reaction $^7\mathrm{Be}(p,\gamma)^8\mathrm{B}$ are free of short-distance counterterms at LO in halo EFT. Thus, these two observables are correlated at this order and a measurement of the charge radius can provide independent information on the S-factor.

Our strategy is twofold: First, we match our low-energy coupling constants to the proton separation energy of 8B and the asymptotic normalization coefficients (ANCs) determined from either ab initio nuclear-structure calculations or from transfer reaction measurements [27–29] in order to calculate both the charge radius of ^{8}B and the S-factor at threshold. Second, we demonstrate the leading-order correlation between these two observables, and we show explicitly how a datum for the charge radius of ^{8}B would put a constraint on the threshold astrophysical S-factor for $^7\mathrm{Be(p,\,\gamma)}^8\mathrm{B}$. In this connection, we employ two different field theories; with and without explicit inclusion of the excited-core state. The incorporation of the excited-core field corresponds to an inclusion of additional short-distance physics, and therefore allows to study the stability of the EFT approach in LO calculations.

The paper is structured as follows. In Sec. II, we introduce the halo EFT for the ^{8}B system. We provide a detailed discussion of the renormalization in a P-wave channel with Coulomb interactions and the relevant low-energy constants at LO. In Sec. III, we calculate the charge form factor of ^{8}B. The radiative capture reaction, $^7\mathrm{Be}(p,\gamma)^8\mathrm{B}$, is considered in Sec. IV, and the correlation between the cross section at threshold and the charge radius

of ^{8}B is discussed in Sec. V. We conclude with a summary and an outlook in Sec. VI. Some properties of the Coulomb Green's function and P-wave integrals are reviewed in the Appendices.

II. HALO EFT FOR P-WAVE INTERACTIONS BETWEEN CHARGED PARTICLES

The $J^\pi = 2^+$ ground state of ^{8}B can be viewed as a halo state consisting of a ($J^\pi = 3/2^-$) ^{7}Be core and a proton that is bound in a relative P-wave. This system is amenable to Halo EFT since it displays a separation of scales. The one-proton separation energy of ^{8}B is $B = 0.1375$ MeV and the energy of the first excited state of the ^{7}Be core is $E^* = 0.4291$ MeV. In our EFT approach, we will include the proton, the ground-state ^{7}Be-core and its first excited state as explicit degrees of freedom. An estimate for the breakdown scale of this EFT is given by the lowest state not included within this theory. Since the energy of the second excited state of ^{7}Be is relatively high, at 4.57 MeV, the relevant high-energy breakdown scale is rather the threshold for breakup of ^{7}Be into ^{3}He and ^{4}He at $E_\alpha = 1.5866$ MeV [33].

The Lagrangian for this system, including the P-wave interaction between the proton and the ^{7}Be core ground and excited state, is given by [26]

$$\begin{aligned}
\mathcal{L} =& \mathrm{p}^\dagger_\sigma \Big(i\mathrm{D}_t + \frac{\mathbf{D}^2}{2m} \Big) \mathrm{p}_\sigma + \mathrm{c}^\dagger_a \Big(i\mathrm{D}_t + \frac{\mathbf{D}^2}{2M} \Big) \mathrm{c}_a \\
&+ \tilde{\mathrm{c}}^\dagger_\sigma \Big(i\mathrm{D}_t + \frac{\mathbf{D}^2}{2M} - E^* \Big) \tilde{\mathrm{c}}_\sigma + \mathrm{d}^\dagger_\alpha \Big[\Delta + \nu \Big(i\mathrm{D}_t + \frac{\mathbf{D}^2}{2M_{\rm tot}} \Big) \Big] \mathrm{d}_\alpha \\
&- g_1 \Big[\mathrm{d}^\dagger_\alpha \mathcal{C}^\alpha_{jk} \mathcal{C}^j_{a\sigma} \mathrm{c}_a \left((1-f) i \overrightarrow{\nabla}_k - f i \overleftarrow{\nabla}_k \right) \mathrm{p}_\sigma + \mathrm{h.c.} \Big] \\
&- g_2 \Big[\mathrm{d}^\dagger_\alpha \mathcal{C}^\alpha_{\beta k} \mathcal{C}^\beta_{a\sigma} \mathrm{c}_a \left((1-f) i \overrightarrow{\nabla}_k - f i \overleftarrow{\nabla}_k \right) \mathrm{p}_\sigma + \mathrm{h.c.} \Big] \\
&- g_* \Big[\mathrm{d}^\dagger_\alpha \mathcal{C}^\alpha_{jk} \mathcal{C}^j_{\sigma\chi} \tilde{\mathrm{c}}_\chi \left((1-f) i \overrightarrow{\nabla}_k - f i \overleftarrow{\nabla}_k \right) \mathrm{p}_\sigma + \mathrm{h.c.} \Big] + \dots \,, \qquad (2)
\end{aligned}$$

where p^σ denotes the spin-1/2 proton field with mass m, c^a ($\tilde{\mathrm{c}}^a$) the ^{7}Be core with spin-3/2 (spin-1/2 excited state) field with mass M. The parameter f denotes the mass ratio $m/M_{\rm tot}$, where $M_{\rm tot} = M + m$. The covariant derivatives are defined as $\mathrm{D}_\mu = \partial_\mu + ie\hat{\mathrm{Q}}A_\mu$, where $\hat{\mathrm{Q}}$ is the charge operator. The halo field d_α describing the ^{8}B halo state has mass $M_{\rm tot}$, while the residual mass Δ is needed for renormalization. The signature $\nu = \pm 1$ will be chosen to reproduce the correct effective range [5].

The vertices where the halo field breaks up into a proton and a core have strengths g_1 and

g_2 for the $S = 1, 2$ spin-channels, respectively. Furthermore, the vertex where the halo field breaks up into a proton and an excited core in the $S = 1$ channel has strength g_*. We define the gound-state core coupling $g^2 = g_1^2 + g_2^2$, since the $S = 1, 2$ channels will always appear together in this combination for the observables that we consider. At LO, we have therefore the three independent coupling constants Δ, g and g_*, whose values will be determined by the proton separation energy of ^{8}B and two additional pieces of information on the ^{7}Be core-proton and ^{7}Be excited-state-proton systems. The Clebsch-Gordan coefficients in Eq. (2) are defined as $\mathcal{C}^{\alpha}_{\beta k} = \left(2\beta 1k \middle| (21)\, 2\alpha\right)$, $\mathcal{C}^{\alpha}_{jk} = \left(1j1k \middle| (11)\, 2\alpha\right)$, $\mathcal{C}^{\beta}_{a\sigma} = \left(\frac{3}{2} a \frac{1}{2}\sigma \middle| \left(\frac{3}{2}\frac{1}{2}\right) 2\beta\right)$, $\mathcal{C}^{j}_{a\sigma} = \left(\frac{3}{2} a \frac{1}{2}\sigma \middle| \left(\frac{3}{2}\frac{1}{2}\right) 1j\right)$ and $\mathcal{C}^{j}_{\sigma\chi} = \left(\frac{1}{2}\sigma \frac{1}{2}\chi \middle| \left(\frac{1}{2}\frac{1}{2}\right) 1j\right)$. The combinations $\mathcal{C}^{\alpha}_{jk}\mathcal{C}^{j}_{a\sigma}$, $\mathcal{C}^{\alpha}_{\beta k}\mathcal{C}^{\beta}_{a\sigma}$ and $\mathcal{C}^{\alpha}_{jk}\mathcal{C}^{j}_{\sigma\chi}$, where repeated indices imply summation, give the two spin channels $S = 1, 2$ with the ground-state core and the $S = 1$ channel for the excited core state. The gradient ∇_k in the P-wave interaction vertex is understood to be written as a spherical tensor, that is $\nabla_{-1} = (\nabla_x - i\nabla_y)/\sqrt{2}$, $\nabla_0 = \nabla_z$ and $\nabla_1 = (\nabla_x + i\nabla_y)/\sqrt{2}$. The possible values of the spin indices are: $\alpha, \beta = -2, -1, 0, 1, 2$, $a = -\frac{3}{2}, -\frac{1}{2}, \frac{1}{2}, \frac{3}{2}$, $i, j, k = -1, 0, 1$ and $\sigma, \chi = -\frac{1}{2}, \frac{1}{2}$. The terms included in the Lagrangian above are the relevant pieces to describe all observables at leading order in the low-energy expansion while the ellipsis in Eq. (2) denote the operators required to go beyond leading order.

An important ingredient of our approach is that we include the Coulomb interaction between the proton and the core to all orders by using the Coulomb Green's function $G_{\rm C}$. In terms of Coulomb wavefunctions $\psi_{\mathbf{p}}(\mathbf{r})$, see Appendix A, we can write $G_{\rm C}$ in coordinate space as

$$(\mathbf{r}_1|G_{\rm C}(E)|\mathbf{r}_2) = \int \frac{{\rm d}^3p}{(2\pi)^3} \frac{\psi_{\mathbf{p}}(\mathbf{r}_1)\psi^*_{\mathbf{p}}(\mathbf{r}_2)}{E - \mathbf{p}^2/(2m_{\rm R}) + i\varepsilon} \ , \tag{3}$$

where $m_{\rm R} = mM/M_{\rm tot}$ is the reduced mass. Note that we are using round brackets to indicate coordinate-space states.

A. The irreducible self-energy

To describe the halo bound state, ^{8}B, we need the irreducible self-energy, which is given in terms of Feynman diagrams in Fig. 1. There are two contributions from (i) the core-proton bubble Σ and (ii) the excited core-proton bubble Σ_*. The self energy is required for the full form of the dressed halo propagator and the resulting LSZ-factor for the halo bound state.

The first contribution with the ground-state core field, Σ, is proportional to two powers

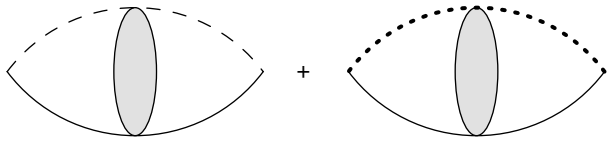

Figure 1: Irreducible self-energy loop-diagrams. The solid line represents the proton, the dashed line the core, and the dotted line the excited-core field. The shaded blob indicates the Coulomb Green's function.

of the P-wave vertex $i(g_1\mathcal{C}^\alpha_{ji}\mathcal{C}^j_{\sigma a}k_i + g_2\mathcal{C}^\alpha_{\beta i}\mathcal{C}^\beta_{\sigma a}k_i)$. As a function of spin-state indices, the irreducible self-energy $\Sigma^{\alpha\beta}$ is diagonal. For convenience, we therefore define $\Sigma = \delta^{\alpha\beta}\Sigma^{\alpha\beta}/5$, and note that the P-wave vertex, squared and summed over spin indices evaluates to

$$\frac{1}{5}\Big(g_1\mathcal{C}^\alpha_{ji}\mathcal{C}^j_{\sigma a}k_i + g_2\mathcal{C}^\alpha_{\beta i}\mathcal{C}^\beta_{\sigma a}k_i\Big)\Big(g_1\mathcal{C}^\alpha_{j'i'}\mathcal{C}^{j'}_{\sigma a}k'_{i'} + g_2\mathcal{C}^\alpha_{\beta' i'}\mathcal{C}^{\beta'}_{\sigma a}k'_{i'}\Big) = \frac{1}{3}(g_1^2+g_2^2)\mathbf{k}\cdot\mathbf{k}' \ . \tag{4}$$

We remind the reader that for all observables considered in this paper, the couplings g_1 and g_2 will always appear in the combination $g^2 = g_1^2 + g_2^2$.

In the following, we will require some specific properties of the Coulomb functions reviewed in the Appendices. Evaluating the irreducible self-energy for the ground state core field using Eq. (B11), we find

$$\begin{aligned} i\Sigma(E) &= i\frac{g^2}{3}\int\frac{\mathrm{d}^3k_1\mathrm{d}^3k_2}{(2\pi)^6}\mathbf{k}_2\cdot\mathbf{k}_1\langle\mathbf{k}_2|G_{\rm C}(E)|\mathbf{k}_1\rangle \\ &= i\frac{g^2}{3}\int\frac{\mathrm{d}^3p}{(2\pi)^3}\frac{\mathbf{X}(E_\mathbf{p})\cdot\mathbf{X}^*(E_\mathbf{p})}{E-\mathbf{p}^2/(2m_{\rm R})} \ . \end{aligned} \tag{5}$$

The properties of the vector function $\mathbf{X}(E_\mathbf{p}) = \int\mathrm{d}^3k\,\mathbf{k}\psi_\mathbf{p}(\mathbf{k})/(2\pi)^3$, where $\psi_\mathbf{p}$ is the Coulomb wavefunction are discussed in detail in Appendix B (cf. Eq. (B1)). Writing $k^2 = 2m_{\rm R}E$ and using Eqs. (B11) and (A11), we obtain the integral,

$$\begin{aligned} i\Sigma(E) &= -i\frac{g^2m_{\rm R}}{3\pi^2}\int\mathrm{d}p\,\frac{C(1,\eta')^2p^4}{p^2-k^2} \\ &= -i\frac{g^2m_{\rm R}}{3\pi^2}\int\mathrm{d}p\,C^2_{\eta'}\Big[p^2+k^2+k_{\rm C}^2+\frac{k_{\rm C}^2k^2+k^4}{p^2-k^2}\Big] \\ &= -ig^2\Big[L_3+(k_{\rm C}^2+k^2)L_1+(k_{\rm C}^2k^2+k^4)J^{\rm fin}(k)\Big] \ , \end{aligned} \tag{6}$$

where we have defined

$$L_n = \frac{m_{\rm R}}{3\pi^2}\int\mathrm{d}p\,C^2_{\eta'}p^{n-1} \tag{7}$$

and

$$J^{\rm fin}(k) = \frac{m_{\rm R}}{3\pi^2}\int\mathrm{d}p\,\frac{C^2_{\eta'}}{p^2-k^2} \ . \tag{8}$$

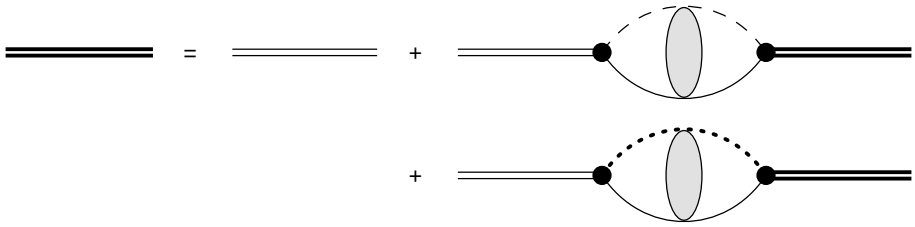

Figure 2: Integral equation for the full halo propagator. The thick (thin) double line denotes the full (bare) halo propagator.

The L_n are formally infinite integrals that we will absorb in the coupling constants Δ and g. Here we have introduced the Sommerfeld factor $C_{\eta'}^2 = 2\pi\eta'/(\exp(2\pi\eta') - 1)$, with $\eta' = k_{\rm C}/p$, and the Coulomb momentum $k_{\rm C} = Z_{\rm c}\alpha m_{\rm R}$, which is the inverse Bohr radius of the system, with $Z_{\rm c}$ the charge number of the core.

The second contribution Σ_*, computed from the loop diagram involving the excited core field, is given by

$$i\Sigma_*(E) = -ig_*^2\Big[L_3 + (k_{\rm C}^2 + k_*^2)L_1 + (k_{\rm C}^2 k_*^2 + k_*^4)J^{\rm fin}(k_*)\Big] \ , \tag{9}$$

where $k_* = \sqrt{2m_{\rm R}(E - E^*)}$.

We can evaluate the finite integral $J^{\rm fin}$ using the integral representation of the polygamma function ψ [30]. Writing $\eta = k_{\rm C}/k$, we have

$$\begin{aligned} \psi(i\eta) + \frac{1}{2i\eta} - \log(i\eta) &= -2\int_0^\infty {\rm d}\eta' \frac{\eta'}{\eta'^2 - \eta^2}\frac{1}{\exp(2\pi\eta') - 1} &(10)\\ &= \frac{k^2}{\pi k_{\rm C}}\int_0^\infty {\rm d}p \frac{1}{p^2 - k^2}\frac{2\pi k_{\rm C}/p}{\exp(2\pi k_{\rm C}/p) - 1} \\ &= \frac{3\pi k^2}{k_{\rm C} m_{\rm R}} J^{\rm fin}(k) \ , &(11)\end{aligned}$$

and thus

$$J^{\rm fin}(k) = \frac{k_{\rm C}}{6\pi E}\Big(\psi(i\eta) + \frac{1}{2i\eta} - \log i\eta\Big) \ . \tag{12}$$

This completes the calculation of the self energy.

B. Elastic proton-core scattering

The low-energy coupling constants can be related to the effective-range parameters of elastic proton-^{7}Be scattering. To achieve this, we first need to write down the full halo propagator with the self-energy bubble summed to all orders.

The bare propagator $D_{\rm bare}$ in its center of mass frame is given by

$$iD_{\rm bare}(E) = \frac{i}{\Delta + \nu E + i\varepsilon} \ , \tag{13}$$

and the full propagator is given by the geometric series

$$iD(E) \ = \ iD_{\rm bare}(E) + iD_{\rm bare}(E)\, i\left[\Sigma(E) + \Sigma_*(E)\right]\, iD(E) \ , \tag{14}$$

which is also shown schematically in Fig. 2. It can be written in closed form as

$$\begin{aligned} iD(E) &= \frac{iD_{\rm bare}(E)}{1 + \left[\Sigma(E) + \Sigma_*(E)\right] D_{\rm bare}(E)} \\ &= \frac{i}{\Delta + \nu E + \Sigma(E) + \Sigma_*(E) + i\varepsilon} \ . \end{aligned} \tag{15}$$

Note that the full halo field propagator is given in terms of irreducible self-energy bubbles from both the ground-state core field Σ and the excited-state core field Σ_*.

The elastic scattering t-matrix T_1 is obtained by enclosing the core-proton propagator with incoming (–) and outgoing (+) Coulomb wavefunctions as shown in Fig. 3. Using the expressions from Eq. (B11), for the P-wave integrals with the Coulomb wavefunctions, T_1 is given by

$$\begin{aligned} iT_1(E) &= ig^2 D(E)\ (\mathbf{X}^+(E))^* \cdot \mathbf{X}^-(E) \\ &= ig^2 D(E) \exp\left(2i\sigma_1\right) p^2 C(1,\eta)^2 \ , \end{aligned} \tag{16}$$

where the P-wave pure Coulomb phaseshift is given by σ_1. The t-matrix is given in terms of observables according to

$$T_1(E) = \frac{6\pi}{m_{\rm R}} \frac{k^2 \exp\left(2i\sigma_1\right)}{k^3(\cot\delta_1 - i)} \ , \tag{17}$$

where δ_1 denotes the P-wave phaseshift due to the strong interaction. We can then match Eqs. (16) and (17) to arrive at

$$k^3 C(1,\eta)^2(\cot\delta_1 - i) = \frac{6\pi}{m_{\rm R}} \left[g^2 D(E)\right]^{-1} \ . \tag{18}$$

The Coulomb-modified effective range expansion (ERE) for the P-wave proton-^{7}Be system, with both the ground state and excited state core fields included, is [31]

$$k^3 C(1,\eta)^2(\cot\delta_1 - i) + 2k_{\rm C} h_1(\eta) + \frac{g_*^2}{g^2} 2k_{\rm C} h_1(\eta_*) = -\frac{1}{a_1} + \frac{1}{2} r_1 k^2 + \dots \ , \tag{19}$$

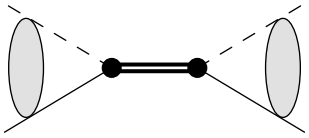

Figure 3: Elastic scattering amplitude for two charged particles with the Coulomb interaction included to infinite order. The intermediate thick double line indicates the full halo propagator.

where $\eta_* = k_{\rm C}/k_*$ and the function h_l is defined as

$$h_l(\eta) = k^{2l}\frac{C(l,\eta)^2}{C(0,\eta)^2}\Big(\psi(i\eta) + \frac{1}{2i\eta} - \log(i\eta)\Big) \ , \tag{20}$$

with ψ being the polygamma function. For $l = 1$, this reduces to

$$h_1(\eta) = k^2(1+\eta^2)\Big(\psi(i\eta) + \frac{1}{2i\eta} - \log(i\eta)\Big) = \frac{3\pi}{m_{\rm R}k_{\rm C}}k^4(1+\eta^2)J^{\rm fin}(E) \ , \tag{21}$$

where Eq. (12) has been used in the last step.

Combining Eqs. (18) and (19) and using that the $J^{\rm fin}$ and h_1 terms cancel out, we match order by order in k^2 to obtain

$$a_1 \ = \ -\frac{m_{\rm R}}{6\pi}\left[\frac{\Delta}{g^2} - \left(1+\frac{g_*^2}{g^2}\right)L_3 - \left(k_{\rm C}^2 + k_{\rm C}^2\frac{g_*^2}{g^2} - 2m_{\rm R}E^*\frac{g_*^2}{g^2}\right)L_1\right]^{-1} \ , \tag{22}$$

$$r_1 \ = \ \frac{12\pi}{m_{\rm R}}\left[\frac{\nu}{2m_{\rm R}g^2} - \left(1+\frac{g_*^2}{g^2}\right)L_1\right] \ . \tag{23}$$

These are the P-wave scattering parameters for the $J = 2$ channel. Equations (22) and (23) define the two renormalization conditions needed in the case of a P-wave interaction in the presence of the Coulomb interaction. The Coulomb-modified ERE contains the ratio of g^2 and g_*^2. We note that these are both inversely proportional to the wavefunction renormalization or LSZ factor $\mathcal{Z}$ of the full halo propagator and their ratio is therefore finite.

The wavefunction renormalization $\mathcal{Z}$ is the residue of the halo propagator at the bound state pole. We can thus calculate $\mathcal{Z}$ as

$$\begin{aligned}
\mathcal{Z} \ &= \ \Big[\frac{{\rm d}(D^{-1})}{{\rm d}E}\Big]^{-1}\Big|_{E=-B} \\
&= \ \Big[\nu + \Sigma' + \Sigma'_*\Big]^{-1}\Big|_{E=-B} \qquad (24) \\
&= \ \frac{6\pi}{g^2 m_{\rm R}^2}\left[r_1 - \frac{2k_{\rm C}}{m_{\rm R}}\frac{\rm d}{{\rm d}E}\left(h_1(\eta) + \frac{g_*^2}{g^2}h_1(\eta_*)\right)\right]^{-1}\Big|_{E=-B} \ , \qquad (25)
\end{aligned}$$

Table I: Asymptotic Normalization Coefficients (ANCs) calculated by Nollett and Wiringa [27] and Zhang *et al.* [26], by Navrátil *et al.* [28], and extracted from a proton-transfer reaction by Tabacaru et al. [29]. The ANCs are given in $\mathrm{fm}^{-1/2}$ for the two spin-channels $S = 1, 2$ (A_1, A_2) and for the $S = 1$ channel with an excited core (A_*).

Ref.	A_1	A_2	A_*
"Nollett" [27], [26]	$-0.315(19)$	$-0.662(19)$	0.3485(51)
"Navrátil" [28]	-0.294	-0.650	–
"Tabacaru" [29]	0.294(45)	0.615(45)	–

where we have used Eqs. (15), (6), (9) and (23).

C. Matching to the Asymptotic Normalization Coefficients

Above, we derived matching conditions that relate the low-energy coupling constants Δ and g, g_* to the parameters of the Coulomb-modified ERE. In practice, we require the one-proton separation energy and the effective range as input for our calculations. However, we can also obtain the effective range from the Asymptotic Normalization Coefficients (ANCs), which are defined as the coefficient of the bound-state wavefunction outside the range R of the interaction. In this exterior region, the solution to the radial wavefunction $w(r)$ is proportional to a Whittaker W-function in the Coulomb case. We can therefore write

$$w_l(r) = AW_{-i\eta,l+1/2}(2\gamma r) \ , \quad \text{for} \quad r > R \ , \tag{26}$$

with the binding momentum $\gamma = \sqrt{2m_{\mathrm{R}}B}$ and the coefficent A defining the ANC.

The P-wave effective range for the $J = 2$ channel is then obtained by using the ANCs either from *ab initio* microscopic calculations, or from a transfer reaction experiment. In this work, we compare three different sets of input ANCs given in Table I. Firstly, we employ ANCs from variational Monte Carlo calculations by Nollett and Wiringa [27] and by Zhang et al. [26] for the excited-core channel. Secondly, we employ ANCs from an NCSM/RGM calculation by Navrátil et al. [28]. In this case, no error estimate was provided for the published result. Finally, we use ANCs extracted from a proton-transfer experiment by Tabacaru et al. [29]. These three sets of ANCs are denoted "Nollett", "Navrátil", and

"Tabacaru", respectively, and are listed in Table I. To obtain the effective range from the ANCs we use the relation derived by König *et al.* in Ref. [32][1]. For the ground state ANCs we obtain

$$A_1^2 + A_2^2 = 2\gamma^2\Gamma(2+k_{\rm C}/\gamma)^2\left[-r_1 + \frac{2k_{\rm C}}{m_{\rm R}}\frac{\rm d}{{\rm d}E}\left(h_1(\eta) + \frac{g_*^2}{g^2}h_1(\eta_*)\right)\Big|_{E=-B}\right]^{-1}, \qquad (27)$$

and for the excited state

$$A_*^2 = 2\gamma_*^2\Gamma(2+k_{\rm C}/\gamma_*)^2\left[-\frac{g^2}{g_*^2}r_1 + \frac{2k_{\rm C}}{m_{\rm R}}\frac{\rm d}{{\rm d}E}\left(\frac{g^2}{g_*^2}h_1(\eta) + h_1(\eta_*)\right)\Big|_{E=-B}\right]^{-1}, \qquad (28)$$

where $\gamma_* = \sqrt{2m_{\rm R}(B+E_*)}$. The two equations (27) and (28) determine the two unknowns g^2/g_*^2 and the effective range r_1. Using the calculated and measured ANCs for ^{8}B in the $S = 1, 2$ channels in Table I, we find the effective range

$$r_1 = \begin{cases} -(60 \pm 4)\ {\rm MeV} & ({\rm Nollett\ ANCs}) \\ -63\ {\rm MeV} & ({\rm Navrátil\ ANCs}\ ) \\ -(69 \pm 13)\ {\rm MeV} & ({\rm Tabacaru\ ANCs}) \end{cases}, \qquad (29)$$

where we have used the excited state ANC calculated by Zhang et al. [26] for all three results. The change in the effective range from including the excited-core state corresponds to an 7-8% increase.

It is important to note that the wave function renormalization of the halo propagator can be expressed directly in terms of the ANCs, according to

$$\mathcal{Z} = -\frac{3\pi}{g^2 m_{\rm R}^2\gamma^2\Gamma(2+k_{\rm C}/\gamma)^2}\left(A_1^2 + A_2^2\right) = -\frac{3\pi}{g_*^2 m_{\rm R}^2\gamma_*^2\Gamma(2+k_{\rm C}/\gamma_*)^2}A_*^2\,. \qquad (30)$$

Both expressions on the right-hand-side give the same value for the $\mathcal{Z}$-factor as one can easily verify by using Eqs. (27) and (28). Note that the LSZ residue in Eq. (30) is proportional to the ground-state ANCs squared. These formulas can be used to make predictions of bound-state properties, without having to extract effective range parameters.

III. THE CHARGE FORM FACTOR

We are now in the position to obtain results for the charge radius of ^{8}B. The charge radius is obtained from the charge form factor $F_{\rm C}$, that can be measured e.g. using elastic

[1] Here we corrected a typographical error in Eq. (85) of Ref. [32].

Figure 4: Feynman diagram for $\Gamma_{\rm tree}$ diagram. The curly (double) line indicates the photon (halo) field.

electron-^{8}B scattering. The charge form factor can be extracted from the matrix element of the zero-component of the electromagnetic current J^μ in the halo nucleus,

$$\langle \mathbf{p}_2 | J^0 | \mathbf{p}_1 \rangle = (Z_{\rm c}+1) e F_{\rm C}(Q) \ , \tag{31}$$

evaluated in the Breit frame. The external photon momentum (or momentum exchange) is given by $\mathbf{Q} = \mathbf{p}_2 - \mathbf{p}_1$, where $\mathbf{p}_1$ ($\mathbf{p}_2$) is the incoming (outgoing) momentum state of the scattered nucleus. Note that we use the standard non-relativistic normalization of one-particle states, $\langle \mathbf{p}_2 | \mathbf{p}_1 \rangle = (2\pi)^3 \delta^3(\mathbf{p}_2 - \mathbf{p}_1)$.

The irreducible diagrams that we need to evaluate for this matrix element are a tree-diagram $\Gamma_{\rm tree}$ with the A_0 photon coupling to the halo field, see Fig. 4, and a loop-diagram $\Gamma_{\rm loop}$ where the A_0 photon couples to either the (excited) core or the proton, see Fig. 5.

We have calculated the charge radius at LO, using both the EFT that contains only the ground state of the core and one that also includes the excited state of the core. This leads to small differences in the result that will be discussed below. Furthermore, we are limited to a LO calculation since at NLO a short-range operator $\mathrm{d}_\alpha^\dagger \nabla^2 A_0 \mathrm{d}_\alpha$ enters, which requires a form factor datum for renormalization.

A. Evaluation of $\Gamma_{\rm tree}$

The photon can couple directly to the halo field at tree level. This diagram, which is shown in Fig. 4, is given by

$$i\Gamma_{\rm tree} = i\nu e (Z_{\rm c}+1) \ . \tag{32}$$

B. Evaluation of $\Gamma_{\rm loop}$

In total we have four loop diagrams contributing to the LO charge form factor. These are shown in Fig. 5. They are loop diagrams in which an external A_0 photon couples either

to the proton, the core or to the excited-core field.

Let us start by writing out the integral for the ground state proton-core loop. The momentum space integral, for momentum transfer $\mathbf{Q}$, is given by

$$\begin{aligned} i\Gamma_{\text{loop,g.s.}}(\mathbf{Q}) = &- i\frac{g^2 eZ_{\text{c}}}{3}\int \frac{\mathrm{d}^3k_1\mathrm{d}^3k_2\mathrm{d}^3k_3}{(2\pi)^9}\mathbf{k}_3\cdot\mathbf{k}_1\langle\mathbf{k}_3|G_{\text{C}}(-B)|\mathbf{k}_2 - f\mathbf{Q}/2\rangle \\ &\times\langle\mathbf{k}_2 + f\mathbf{Q}/2|G_{\text{C}}(-B)|\mathbf{k}_1\rangle \\ &+\Big[(f\to 1-f),\ (Z_{\text{c}}\to 1)\Big]\ , \end{aligned} \tag{33}$$

where $\mathbf{k}_1$ and $\mathbf{k}_3$ are the loop-momenta in the outermost loops in the diagrams in Fig. 5, and $\mathbf{k}_2$ is the loop-momentum in the middle loop. The $[(f\to 1-f),\ (Z_{\text{c}}\to 1)]$ term is present since the photon can couple to both the ground state core field and to the proton. Continuing by doing a Fourier transform on the $\mathbf{k}_2$ momentum, and using Eq. (C7), we write this as

$$\begin{aligned} i\Gamma_{\text{loop,g.s.}}(\mathbf{Q}) = &- i\frac{g^2 eZ_{\text{c}}}{3}\int \frac{\mathrm{d}^3k_1\mathrm{d}^3k_2\mathrm{d}^3k_3}{(2\pi)^9}\mathrm{d}^3r_1\mathrm{d}^3r_2\ \mathbf{k}_3\cdot\mathbf{k}_1\langle\mathbf{k}_3|G_{\text{C}}(-B)|\mathbf{r}_1) \\ &\times\exp\left(i\mathbf{k}_2\cdot(\mathbf{r}_2-\mathbf{r}_1)\right)\exp\left(if\mathbf{Q}\cdot(\mathbf{r}_1+\mathbf{r}_2)/2\right)(\mathbf{r}_2|G_{\text{C}}(-B)|\mathbf{k}_1\rangle \\ &+\Big[(f\to 1-f),\ (Z_{\text{c}}\to 1)\Big] \\ = &- i3g^2 eZ_{\text{c}}\int \mathrm{d}^3r\ \exp\left(if\mathbf{Q}\cdot\mathbf{r}\right)\left|\lim_{r'\to 0}\left(\frac{G_{\text{C}}^{(1)}(-B;r',r)}{r'}\right)\right|^2 \\ &+\Big[(f\to 1-f),\ (Z_{\text{c}}\to 1)\Big]\ . \end{aligned} \tag{34}$$

Replacing the limit of the partial-wave projected Coulomb Green's function by Eq. (A15) we arrive at

$$\begin{aligned} \Gamma_{\text{loop,g.s.}}(Q) = &- \frac{e(Z_{\text{c}}+1)g^2 m_{\text{R}}^2\Gamma(2+k_{\text{C}}/\gamma)^2\gamma^2}{3\pi} \\ &\times\int \mathrm{d}r\ \left[1-\Big((1-f)^2+Z_{\text{c}}f^2\Big)\frac{r^2Q^2}{6(Z_{\text{c}}+1)}+\mathcal{O}(Q^4)\right]W_{-k_{\text{C}}/\gamma,3/2}(2\gamma r)^2\ , \end{aligned} \tag{35}$$

where W is the Whittaker W-function. The order Q^2 integral in Eq. (35) can be solved numerically.

Using the same steps as above we can also derive the contribution from the excited-core

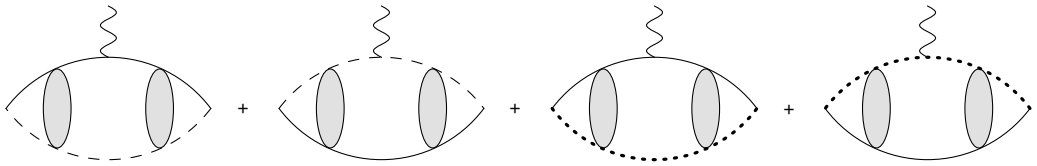

Figure 5: Feynman diagrams for $\Gamma_{\rm loop}$ where the photon couples either to the proton (solid line), the core (dashed line) or excited core (dotted line) in the proton-core loop.

diagrams

$$\Gamma_{\rm loop,e.s.}(Q) = -\frac{e(Z_{\rm c}+1)g_*^2 m_{\rm R}^2 \Gamma(2+k_{\rm C}/\gamma_*)^2\gamma_*^2}{3\pi} \times \int {\rm d}r \ \left[1-\left((1-f)^2+Z_{\rm c}f^2\right)\frac{r^2Q^2}{6(Z_{\rm c}+1)}+\mathcal{O}(Q^4)\right] W_{-k_{\rm C}/\gamma_*,3/2}(2\gamma_* r)^2 \ . \tag{36}$$

C. The Charge Radius

The charge radius $r_{\rm C}$ is defined from the Q^2-term in the expansion of the charge form factor in even powers of Q

$$F_{\rm C}(Q) = 1 - \frac{r_{\rm C}^2}{6}Q^2 + \dots \ , \tag{37}$$

which is given by the sum of the three contributions discussed above

$$F_{\rm C}(Q) = \frac{\mathcal{Z}}{e(Z_{\rm c}+1)}\left(\Gamma_{\rm tree}+\Gamma_{\rm loop,g.s.}(Q)+\Gamma_{\rm loop,e.s.}(Q)\right) \ , \tag{38}$$

with $\mathcal{Z}$ the wavefunction renormalization in Eq. (25). We evaluate this expression for $Q=0$ to show that the form factor is normalized correctly. At $Q=0$, $\Gamma_{\rm loop,g.s.}$ in Eq. (33) simplifies to

$$i\Gamma_{\rm loop,g.s.}(0) \ = \ -i\frac{g^2 e(Z_{\rm c}+1)}{3}\int\frac{{\rm d}^3p}{(2\pi)^3}\frac{\mathbf{X}(E_{\mathbf{p}})\cdot\mathbf{X}^*(E_{\mathbf{p}})}{\Big(-B-p^2/(2m_{\rm R})\Big)^2} \ .$$

where we have used the k-space version of Eq. (3), the orthonormality of the Coulomb wavefunctions and Eq. (B1). Now, comparison to Eq. (5) gives

$$\Gamma_{\rm loop,g.s.}(0) = e(Z_{\rm c}+1)\Sigma'(-B) \ . \tag{39}$$

For the excited core contribution we similarly have

$$\Gamma_{\rm loop,e.s.}(0) = e(Z_{\rm c}+1)\Sigma'_*(-B) \ . \tag{40}$$

Table II: The relevant scales and parameters in the ^{8}B system. See text for details.

$k_{\rm C}$	γ	γ_*	r_1	k_α	$1/R_{^7{\rm Be}}$	f	$Z_{\rm c}$
23.79 MeV	14.97 MeV	30.39 MeV	$\sim$ 60-70 MeV	50.86 MeV	74.55 MeV	1/8	4

Equations (39) and (40) together with Eqs. (24), (32) and (38) lead to the correct normalization

$$F_{\rm C}(0) = 1 \ . \tag{41}$$

To obtain the charge radius we first define

$$\Gamma_{\rm loop,g.s.}(Q) + \Gamma_{\rm loop,e.s.}(Q) = \Gamma^{(0)}_{\rm loop} + \Gamma^{(2)}_{\rm loop} Q^2 + \mathcal{O}(Q^4) \tag{42}$$

and use this to expand Eq. (38) in powers of Q^2

$$\begin{aligned} F_{\rm C}(Q) \ &= \ \frac{\mathcal{Z}}{e(Z_{\rm c}+1)} \left(\Gamma_{\rm tree} + \Gamma^{(0)}_{\rm loop} + \Gamma^{(2)}_{\rm loop} Q^2 \right) + \mathcal{O}(Q^4) \\ &= \ 1 + \frac{\mathcal{Z}}{e(Z_{\rm c}+1)} \Gamma^{(2)}_{\rm loop} Q^2 + \mathcal{O}(Q^4) \ , \end{aligned} \tag{43}$$

where we used Eq. (41) in the last step. The charge radius is therefore given by

$$r^2_{\rm C} = -6 \frac{\mathcal{Z}}{e(Z_{\rm c}+1)} \Gamma^{(2)}_{\rm loop} \ . \tag{44}$$

Evaluating the order Q^2 integrals in Eqs. (35) and (36) we arrive at the values

$$r^2_{\rm C} = \begin{cases} (2.56 \pm 0.08 \text{ fm})^2 & \text{(Nollett ANCs)} \\ (2.50 \text{ fm})^2 & \text{(Navrátil ANCs)} \\ (2.41 \pm 0.18 \text{ fm})^2 & \text{(Tabacaru ANCs)} \end{cases} , \tag{45}$$

using the parameter values for the ^{8}B system in Table II and the ANCs of Nollett and Wiringa [27], Navrátil *et al.* [28] and Tabacaru *et al.* [29], and the excited core ANC given in Zhang *et al.* [26].

The errors given in Eq. (45) are due to the uncertainties on the calculated or experimentally extracted ANCs that are used as input. In addition, we obtain an estimate for the LO halo EFT error by assuming that the breakdown scale of the theory is given by the α-threshold of ^{7}Be. It is at $E_\alpha = 1.5866$ MeV [33] which defines a break-down momentum scale $k_{\rm hi} \sim k_\alpha = 50.86$ MeV. The low-momentum scale is defined by the binding momentum

$k_{\rm lo} \sim \gamma = 14.97$ MeV. The expected EFT error for the charge radius squared is therefore $k_{\rm lo}/k_{\rm hi} \sim 30\%$, which is larger than the input ANC errors quoted above.

At the next order, the short-range operator $\mathrm{d}_\alpha^\dagger \nabla^2 A_0 \mathrm{d}_\alpha$ enters the electromagnetic current. The coefficient of this operator can be fit to the charge radius or the charge form factor. We can analyze, however, the stability of the EFT without a full higher order calculation, by only including the minimal set of explicit degrees of freedom at first and then add more physics by adding additional information into the EFT.

If we remove the excited-core field from the EFT we would arrive at the LO result $r_{\rm C}^2 = (2.32 \text{ fm})^2$, using the central value of the ANCs by Nollett and Wiringa [27] only. For such a field theory, an estimate of the break-down scale would be the momentum scale corresponding to the core excited-state energy $\sqrt{2m_{\rm R}E_*} = 26.4$ MeV, and thus the expected EFT error for the charge radius squared would be 57%. Comparing the "Nollett ANCs" charge radius result in Eq. (45), $r_{\rm C} = (2.56 \pm 0.38(\text{EFT}))$ fm, with the result using only the ground state core field $r_{\rm C} = (2.32 \pm 0.67(\text{EFT}))$ fm, we see that the size of expected error decreases due to the inclusion of the excited state of the ^{7}Be core. Therefore, even though we formally only consider LO, we can test the stability of the EFT: The inclusion of additional information at higher energies, *i.e.* shorter distances, leads to a reduction in the anticipated error.

The charge radius of ^{8}B has been calculated by Pastore *et al.* [34] with quantum Monte Carlo techniques. The authors find the point-proton charge radius to be $r_{\rm pt-p} = 2.48$ fm. Folding the point-proton charge radius with the proton and neutron charge radii, and adding relativistic plus spin-orbit corrections as in Ref. [35], gives a charge radius of $r_{\rm C} = 2.60$ fm. This value is compatible with our LO result within the estimated error of 30% for the radius squared.

IV. RADIATIVE CAPTURE

We will now consider low-energy radiative proton capture on ^{7}Be. We will not consider initial-wave scattering due to the strong interaction since it is exponentially suppressed at threshold $E_{\rm c.m.} = 0$ due to the Coulomb repulsion. Note, however, that we do consider pure Coulomb scattering to all orders for the incoming proton-core pair.

Without initial-wave scattering we are left with the diagrams shown in Figs. 6 and 7,

which for the capture process has the direction of time from right to left. Below we discuss these diagrams in detail. Since the bound state is a $J^\pi = 2^+$ due to a P-wave interaction, the E1 capture occurs through an incoming proton-core pair in a relative S- or D-wave, with spin channel either $S = 1$ or $S = 2$. These are the relevant channels since the E1 operator changes the angular momentum by one, and the spin of the constituent ^{7}Be core is $3/2^-$ while the proton has spin $1/2^+$. The two channels are defined by the two different vertices in the Lagrangian Eq. (2), $g_1\mathcal{C}^\alpha_{kj}\mathcal{C}^k_{\sigma a}$ for the spin-1 channel ($k = -1, 0, 1$) and $g_2\mathcal{C}^\alpha_{\beta j}\mathcal{C}^\beta_{\sigma a}$ for the spin-2 channel ($\beta = -2, -1, 0, 1, 2$), where the Clebsch-Gordan coefficients guarantee that the spins of the constituents couple to either $S = 1$ or $S = 2$ and that the total spin couples to the E1 operator to give a $J = 2$ final state. For the threshold capture cross section the S-wave dominates and we therefore drop the D-wave contribution.

The threshold radiative capture cross section without initial wave scattering is purely proportional to the ground state ANCs in the combination $A_1^2 + A_2^2$, since the incoming particles are in their respective ground states. Thus, even though the excited-core field does not contribute to the S-factor result presented here, the excited state is included in the field theory and we may therefore estimate the error from the α-breakup threshold of ^{7}Be. The results we present are at LO, but since the pole-position is fixed by the ANCs, the threshold S-factor should be accurate. This is because the higher-order operators in the field theory will enter with additional powers of the energy. Therefore the error for the threshold S-factor is mainly due to the uncertainty in the input ANCs, while at finite energies the error is from neglected initial-wave interactions, D-wave component and higher-order operators.

The amplitudes presented in this section will have various indices, one from the vector photon A^i and three from the incoming and outgoing particles (α, σ, a). The first index will thus be dotted by the polarization vectors and the remaining (written in parenthesis) will be traced in the summation of $|\mathcal{A}|^2$. Furthermore, the diagrams are evaluated in the zero-momentum frame of the proton and the core. The incoming proton (core) has thus momentum $\mathbf{p}$ $(-\mathbf{p})$. The outgoing photon (halo) has momentum $\mathbf{Q}$ $(-\mathbf{Q})$.

a. Capture diagram with intermediate halo propagator This is the simplest diagram, and is shown in Fig. 6(a). Since the amplitude is proportional to the momentum flowing into the photon-halo field vertex, in Coulomb gauge, then the diagram is identically zero in the zero-momentum frame

$$i\mathcal{A}^{i(\alpha)}_{1(\sigma a)} = 0 \ . \tag{46}$$

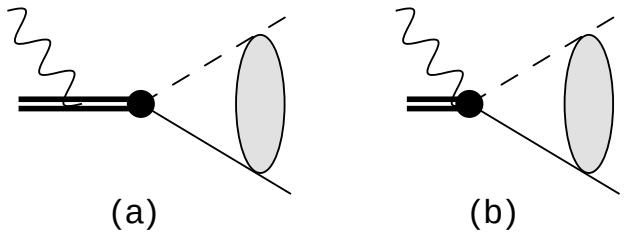

Figure 6: (a) Radiative capture diagram with an intermediate halo propagator. (b) Radiative capture diagram with a photon coupling to the P-wave vertex.

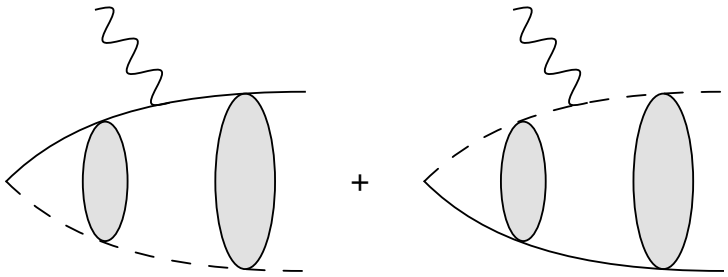

Figure 7: Loop-diagrams for radiative capture. The photon couples either to the proton or the core.

b. Capture diagram with the photon coupling to the P-wave vertex This diagram is given in Fig. 6(b) and is simply

$$\begin{aligned} i\mathcal{A}^{i(\alpha)}_{2(\sigma a)} &= -ie\Big(1-f(Z_{\rm c}+1)\Big)\left(g_1\mathcal{C}^{\alpha}_{ji}\mathcal{C}^{j}_{\sigma a}+g_2\mathcal{C}^{\alpha}_{\beta i}\mathcal{C}^{\beta}_{\sigma a}\right)\int\frac{{\rm d}^3k}{(2\pi^3)}\;\psi_{\mathbf{p}}(\mathbf{k}) \\ &= -ie\Big(1-f(Z_{\rm c}+1)\Big)\left(g_1\mathcal{C}^{\alpha}_{ji}\mathcal{C}^{j}_{\sigma a}+g_2\mathcal{C}^{\alpha}_{\beta i}\mathcal{C}^{\beta}_{\sigma a}\right)\psi_{\mathbf{p}}(0)\;. \end{aligned} \tag{47}$$

The $\psi_{\mathbf{p}}(0)$ factor implies that this amplitude is purely from an incoming S-wave.

c. Capture loop diagrams The loop diagrams contributing to the capture process are shown in Fig. 7 and are written in momentum space as

$$\begin{aligned} i\mathcal{A}^{i(\alpha)}_{3(\sigma a)} \;=\; &\left(g_1\mathcal{C}^{\alpha}_{kj}\mathcal{C}^{k}_{\sigma a}+g_2\mathcal{C}^{\alpha}_{\beta j}\mathcal{C}^{\beta}_{\sigma a}\right)\int\frac{{\rm d}^3k_1{\rm d}^3k_2}{(2\pi)^6}\;ik_2^j\langle\mathbf{k}_2|G_{\rm C}(-B)|\mathbf{k}_1+f\mathbf{Q}\rangle i\frac{feZ_{\rm c}(-k_1^i)}{m_{\rm R}}\psi_{\mathbf{p}}(\mathbf{k}_1) \\ &-\left[(f\to 1-f)\;,\;(Z_{\rm c}\to 1)\right]\;. \end{aligned} \tag{48}$$

It involves an incoming Coulomb wavefunction $\psi_{\mathbf{p}}(\mathbf{k}_1)$, the vector photon-core vertex $ifeZ_{\rm c}(-k_1^i)/m_{\rm R}$, a Coulomb Green's function $G_{\rm C}(-B)$, which defines the propagation down to the bound state, and the P-wave interaction vertex $ik_2^j\left(g_1\mathcal{C}^{\alpha}_{kj}\mathcal{C}^{k}_{\sigma a}+g_2\mathcal{C}^{\alpha}_{\beta j}\mathcal{C}^{\beta}_{\sigma a}\right)$. The photon-proton vertex is given by $i(1-f)ek_1^i/m_{\rm R}$. Fourier transforming to coordinate space and

multiplying with the photon polarization vectors $\epsilon_i^{(n)}$, where $n = 1, 2$ and we have chosen $\epsilon^{(1)} = \hat{x}$, $\epsilon^{(2)} = \hat{y}$ and $\mathbf{Q} = \omega\hat{z}$, we arrive at

$$\begin{aligned}\sum_{i=-1}^{1}\sum_{n=1}^{2} i\epsilon_i^{(n)}\mathcal{A}_{3(\sigma a)}^{i(\alpha)} \;=\; & -\left(g_1\mathcal{C}_{kj}^{\alpha}\mathcal{C}_{\sigma a}^{k} + g_2\mathcal{C}_{\beta j}^{\alpha}\mathcal{C}_{\sigma a}^{\beta}\right)\frac{2feZ_{\rm c}\gamma}{3p}(\hat{x}+\hat{y})^j \exp\left(i\sigma_0\right)\Gamma(2+k_{\rm C}/\gamma) \\ & \times\int {\rm d}r\; rW_{-k_{\rm C}/\gamma,3/2}(2\gamma r)j_0(f\omega r)\partial_r\left(\frac{F_0(k_{\rm C}/p,pr)}{r}\right) \\ & -\left[(f\to 1-f)\;,\;(Z_{\rm c}\to 1)\right]\;, \end{aligned} \tag{49}$$

where we have dropped the incoming D-wave component and a negligible j_2 spherical Bessel function.

d. Resulting S-factor The LO cross section for radiative capture is now given by the sum of contributions discussed above

$$\frac{{\rm d}\sigma}{{\rm d}\Omega} = \frac{m_{\rm R}\omega}{8\pi^2 p}\sum_{\alpha,\sigma a}\sum_{i=-1}^{1}\sum_{n=1}^{2}\left|\sqrt{\mathcal{Z}}\epsilon_i^{(n)}\left(\mathcal{A}_{1(\sigma a)}^{i(\alpha)} + \mathcal{A}_{2(\sigma a)}^{i(\alpha)} + \mathcal{A}_{3(\sigma a)}^{i(\alpha)}\right)\right|^2\;, \tag{50}$$

using the expressions for the amplitudes in Eqs. (46), (47) and (49). Note that the amplitudes in Eq. (50) do not depend on the proton-core scattering effective range. This quantity, which was determined through the ANCs, enters solely through the wavefunction renormalization $\mathcal{Z}$ defined in Eq. (25).

We present the total cross section in terms of the astrophysical S-factor

$$S(E) = E\exp\left(2\pi\eta\right)\sigma_{\rm tot}\;, \tag{51}$$

which is basically defined by the removal of the low-energy exponential suppression C_η^2.

The resulting S-factor is presented in Fig. 8 together with existing low-energy direct-capture data from Refs. [36–43]. The threshold value is

$$S(0) = \begin{cases} (20.0 \pm 1.4)\text{ eV b} & \text{(Nollett ANCs)} \\ 18.9\text{ eV b} & \text{(Navrátil ANCs)} \\ (17.3 \pm 3.0)\text{ eV b} & \text{(Tabacaru ANCs)} \end{cases}\;. \tag{52}$$

The errors given in Eq. (52) are due to the errors in the input ANCs. It is important to note that in the capture process the intrinsic EFT error is smaller than the naively expected one. This matrix element is insensitive to uncertainties in the core-proton P-wave interaction since the incoming core and proton are not in a relative P-wave. Furthermore, the binding energy of the final state is fixed and the Z-factor is directly proportional to the ANCs

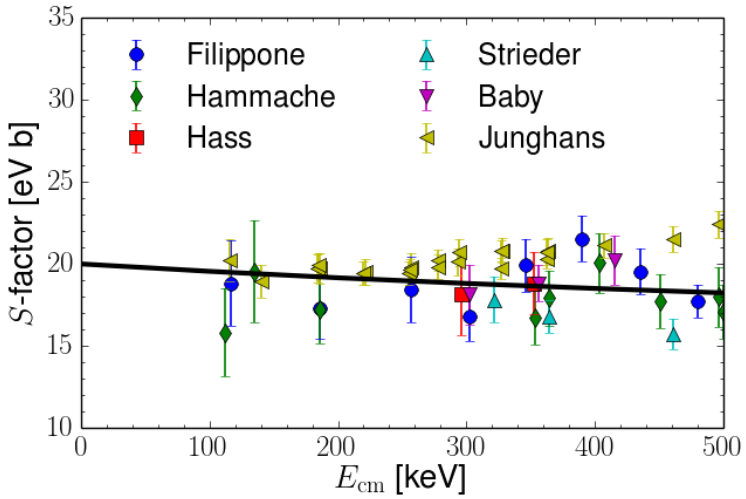

Figure 8: The S-factor of ^{7}Be$(p,\gamma)^8$B as a function of the c.m. energy. The data are from Refs. [36–43]. The solid line is the LO result of this work using input ANCs of Nollett *et al.*.

squared as showed in Eq. (30). Thus, at threshold the only corrections are due to higher-order operators that involve the photon field and these enter with additional powers of the photon energy ω. Momentum and energy conservation implies that $\omega \approx B + \frac{p^2}{2m_{\rm R}}$, where the binding energy scales as $k_{\rm lo}^2$. We therefore estimate the error to be of order $(k_{\rm lo}/k_{\rm hi})^2 \approx 8\%$. These higher-order corrections will, however, influence the shape of the S-factor at larger energies, *i.e.* in the region where comparison with data is possible. This results in an additional uncertainty when attempting extrapolation to threshold energies. Note that this extrapolation uncertainty is much more serious in potential-model descriptions for which the error is not even quantified. Therefore, we present an alternative approach to constrain the threshold S-factor from experimental data: namely to identify its correlation with the previously discussed charge radius of ^{8}B.

V. CORRELATING THE CHARGE RADIUS AND THE THRESHOLD S-FACTOR

At this stage we are able to demonstrate the relationship between the ^{7}Be$(p,\gamma)^8$B S-factor at threshold and the ^{8}B charge radius. Instead of using ground-state ANCs from microscopic calculations or transfer experiments as input, we now let $A_1^2 + A_2^2$ be a free parameter. This parameter is then used to explore correlations between the charge radius of ^{8}B and the

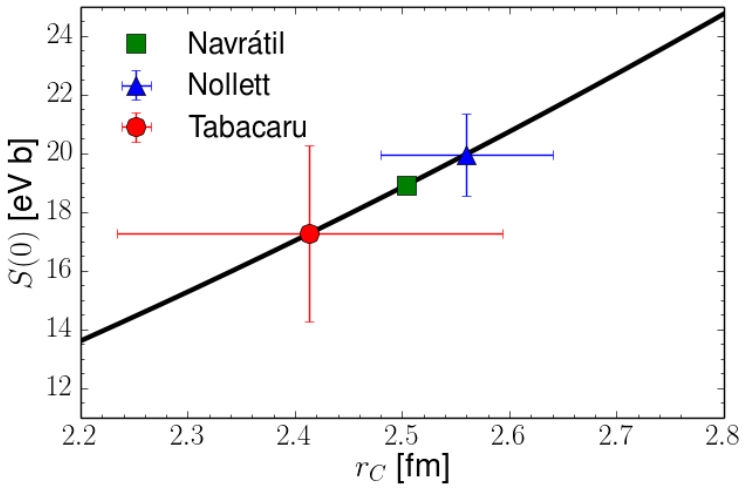

Figure 9: Correlating the threshold S-factor and the charge radius of ^{8}B. The solid line demonstrates the EFT correlation, while the three data points with error bars correspond to results obtained with different input ANCs, either from microscopic ab initio calculations, or from a transfer experiment.

threshold S-factor. However, we still fit the excited state ANC to the result of Zhang *et al.* $A_* = 0.3485(51)$. The resulting correlation plot is shown in Fig. 9. The solid line shows the LO one-parameter correlation predicted by halo EFT. The triangle, square and circle show our results for the S-factor with the input ANCs from Nollett, Navrátil and Tabacaru, respectively. They appear in different positions on the correlation line since changing the ANC leads to a different effective range and thus a different charge radius. In turn, the correlation can be used to constrain the ANC from charge radius measurements.

VI. SUMMARY

In this paper, we have calculated the charge radius and the S-factor for radiative proton capture on ^{7}Be at LO in halo EFT. The parameters required to fix the proton-core interaction were obtained from experiment, or from ab initio calculations. Our prediction for the S-factor at threshold is in agreement with the most recent recommended value for this observable [1] and the EFT calculation by Zhang, Nollett and Phillips [26]. By performing calculations with and without the excited state of ^{7}Be, and thereby changing the amount of microscopic physics included in the EFT, we have tested the stability of our calculation. Furthermore,

we have derived a number of universal expressions that can be applied to any proton halo system bound through resonant p-wave interactions.

If the one-proton separation energy of ^{8}B is kept fixed, the charge radius is directly correlated to the S-factor at threshold at this order in the calculation. A measurement of the S-factor therefore determines not only the ANCs of the ^{7}Be-proton system but also the charge radius. This result provides an excellent example how different observables constrain each other. Note however, that this direct correlation does not exist at the next order in the EFT expansion since two additional counterterms enter. The first counterterm fixes the next contribution in the ERE of ^{7}Be-proton scattering. The second counterterm comes from an operator that couples the photon to the full halo field. Both counterterms could be fitted to the charge form factor, either obtained through a measurement or from an ab initio calculation. This connection to the charge form factor is particularly useful for the latter case since calculations of *static* nuclear properties are generally simpler than reactions or scattering observables. A higher order analysis would thus provide additional constraints on the threshold S-factor and does not directly depend on a measurement of the capture cross section and a subsequent extrapolation.

It is worth noting that the additional counterterm appearing in the electromagnetic current is an inherent limitation for any cluster model that tries to describe charge radii as it accounts for microscopic physics not determined by core-proton scattering properties. Previous calculations using cluster models have tried to circumvent this limitation by taking additional microscopic physics such as core swelling into account, see e.g. [44]. However, the model-dependence of such approaches has not been studied and involves uncontrolled errors. Our EFT approach can therefore provide lower error bounds on any cluster model that employs the same number of degrees of freedom.

Acknowledgments

We thank D. R. Phillips and H. Esbensen for useful discussions. This research was supported in part by the Swedish Research Council (dnr. 2010-4078), the European Research Council under the European Community's Seventh Framework Programme (FP7/2007-2013) / ERC grant agreement no. 240603, the BMBF under grant 05P12PDFTE, the DFG through SFB 634, the Office of Nuclear Physics, U.S. Department of Energy under contract no.

DE-AC02-06CH11357 and by the Helmholtz Association under contract HA216/EMMI. We express our appreciation to the Extreme Matter Institute at GSI and the Institute for Nuclear Theory in Seattle, where part of this work was carried out.

Appendix A: Coulomb wavefunctions and Green's function

We define the Coulomb wavefunction through its partial wave expansion

$$\psi_{\mathbf{k}}(\mathbf{r}) = \sum_{l=0}^{\infty} \phi_l(\eta,\rho) P_l(\hat{\mathbf{k}}\cdot\hat{\mathbf{r}}) \ , \tag{A1}$$

with

$$\phi_l(\eta,\rho) = (2l+1) i^l \exp\left(i\sigma_l(\eta)\right) \frac{F_l(\eta,\rho)}{\rho} \ , \tag{A2}$$

and the Coulomb phase shift $\sigma_l = \arg\Gamma(l+1+i\eta)$. Here we have used the definitions $\rho = kr$ and $\eta = k_{\rm C}/k$, with the Coulomb momentum $k_{\rm C} = Z_{\rm c}\alpha m_{\rm R}$. The regular Coulomb wavefunctions F_l can be expressed in terms of the Whittaker M function through

$$F_l(\eta,\rho) = A(l,\eta) M_{i\eta,l+1/2}(2i\rho) \ , \tag{A3}$$

with

$$A(l,\eta) = \frac{1}{2} \frac{\Gamma(l+1+i\eta)\exp\Big(-\pi\eta/2 - i(l+1)\pi/2\Big)}{(2l+1)!} \ . \tag{A4}$$

We also give the irregular Coulomb wavefunctions G_l in terms of the Whittaker M and W functions as

$$G_l(\eta,\rho) = iF_l(\eta,\rho) + B_l(\eta) W_{i\eta,l+1/2}(2i\rho) \ , \tag{A5}$$

with

$$B_l(\eta) = \frac{\exp\left(\pi\eta/2 + il\pi/2\right)}{\arg\Gamma(l+1+i\eta)} \ . \tag{A6}$$

Moreover, we have defined

$$|\Gamma(l+1+i\eta)|^2 = \Gamma(l+1+i\eta)\Gamma(l+1-i\eta) \tag{A7}$$

and

$$\arg\Gamma(l+1+i\eta) = \sqrt{\frac{\Gamma(l+1+i\eta)}{\Gamma(l+1-i\eta)}} \ , \tag{A8}$$

such that our expressions make sense for imaginary momentum corresponding to bound states.

The Sommerfeld factor is given by

$$C_\eta^2 = C(0,\eta)^2 \;=\; \frac{2\pi\eta}{\exp(2\pi\eta)-1} = \exp(-\pi\eta)\Gamma(1+i\eta)\Gamma(1-i\eta)\;, \tag{A9}$$

and we will also be needing its generalization to higher partial waves

$$C(l,\eta)^2 = \exp(-\pi\eta)\Gamma(l+1+i\eta)\Gamma(l+1-i\eta)\;. \tag{A10}$$

Note in particular that

$$C(1,\eta)^2 = (1+\eta^2)C_\eta^2\;. \tag{A11}$$

The partial wave projected Coulomb Green's function for a bound state is given by

$$G_{\rm C}^{(l)}(E;r,r') \;=\; -\frac{m_{\rm R}p}{2\pi}\frac{F_l(\eta,\rho')\Big[iF_l(\eta,\rho)+G_l(\eta,\rho)\Big]}{\rho'\rho}\;, \tag{A12}$$

that is a product of two linear combinations of Coulomb wavefunctions satisfying the bound state boundary conditions both at zero and infinite separation. The normalization of the Coulomb Green's function Eq. (A12) is set by the Coulomb-Schrödinger equation and the Wronskian of the Coulomb wavefunctions.

Using the identity

$$iF_l(\eta,\rho)+G_l(\eta,\rho) = \exp(i\sigma_l+\pi\eta/2-li\pi/2)W_{-i\eta,l+1/2}(-2i\rho) \tag{A13}$$

and the limit

$$\lim_{r\to 0}\left(\frac{F_1(\eta,\rho)}{\rho^2}\right) = \frac{1}{3}\exp(-\pi\eta/2)\sqrt{\Gamma(2+i\eta)\Gamma(2-i\eta)}\;, \tag{A14}$$

we can then write

$$\lim_{\rho'\to 0}\left(\frac{G_{\rm C}^{(1)}(E;r',r)}{\rho'}\right) = i\frac{m_{\rm R}p}{6\pi}\Gamma(2+i\eta)\frac{W_{-i\eta,3/2}(-2i\rho)}{\rho}\;. \tag{A15}$$

The expression Eq. (A15) is used to evaluate the loop-integrals for the charge form factor and the radiative capture cross section.

Appendix B: P-wave Integrals

When we calculate loop diagrams with P-wave interactions, we have to evaluate integrals that involve Coulomb wavefunctions. In this Appendix, we derive a few useful identities for these calculations.

The most basic constituent of the integrals that we need to solve is the vector integral

$$\mathbf{X}(E_{\mathbf{p}}) = \int \frac{\mathrm{d}^3k}{(2\pi)^3}\mathbf{k}\psi_{\mathbf{p}}(\mathbf{k}) \ . \tag{B1}$$

We will evaluate this integral by performing a Fourier transform of $\psi_{\mathbf{p}}(\mathbf{k})$ to position space followed by a partial integration:

$$\begin{aligned}\mathbf{X}(E_{\mathbf{p}}) \ &= \ \int \frac{\mathrm{d}^3k}{(2\pi)^3}\mathbf{k}\psi_{\mathbf{p}}(\mathbf{k}) = \int \mathrm{d}^3r\psi_{\mathbf{p}}(\mathbf{r})(-i\nabla)\delta^{(3)}(\mathbf{r}) \\ &= \ i\int \mathrm{d}^3r\delta^{(3)}(\mathbf{r})\Big(\nabla\psi_{\mathbf{p}}(\mathbf{r})\Big) \ . \end{aligned} \tag{B2}$$

We will now temporarily fix $\mathbf{p} = p\hat{z}$ and do a partial wave expansion of the Coulomb wavefunction. The derivative in Eq. (B2) is then evaluated to (we are suppressing the η' and ρ dependencies)

$$\nabla\psi_{\mathbf{p}}(\mathbf{r}) = \sum_{l=0}^{\infty}\Big[\hat{r}p\partial_\rho\phi_l P_l(\cos\theta) + \hat{\theta}\frac{p}{\rho}\phi_l\partial_\theta P_l(\cos\theta)\Big] \tag{B3}$$

Note that for $l = 0$ we get

$$\nabla\psi_{\mathbf{p}}(\mathbf{r})\Big|_{l=0} = \hat{r}p\partial_\rho\phi_0 \ , \tag{B4}$$

which is an odd function of $\mathbf{r}$. This means that the integration of the $l = 0$ term is zero. Furthermore, we have

$$\lim_{\rho\to 0}\partial_\rho\phi_l = 0 \ , \ l > 1 \ , \tag{B5}$$

and

$$\lim_{\rho\to 0}\frac{\phi_l}{\rho} = 0 \ , \ l > 1 \ , \tag{B6}$$

which means that only the $l = 1$ term will contribute to $\mathbf{X}$:

$$\begin{aligned}\mathbf{X}(E_{\mathbf{p}}) \ &= \ i\lim_{\rho\to 0}\Big(\cos(\theta)\hat{r}p\partial_\rho\phi_1 - \sin(\theta)\hat{\theta}p\frac{\phi_1}{\rho}\Big) \\ &= \ i\mathbf{p}\lim_{\rho\to 0}\Big(\frac{\phi_1(\eta',\rho)}{\rho}\Big) \ . \end{aligned} \tag{B7}$$

In the last step we used that

$$\cos(\theta)\hat{r} - \sin(\theta)\hat{\theta} = \hat{z} \tag{B8}$$

and that the limits of $\partial_\rho\phi_1$ and ϕ_1/ρ can be written as

$$\lim_{\rho\to 0}\left(\partial_\rho\phi_1(\eta',\rho)\right) = \lim_{\rho\to 0}\Big(\frac{\phi_1(\eta',\rho)}{\rho}\Big) \ . \tag{B9}$$

We can also write this limit using the Sommerfeld factor

$$\lim_{\rho\to 0}\Big(\frac{\phi_1(\eta',\rho)}{\rho}\Big) = i\exp(i\sigma_1)C(1,\eta')\ , \tag{B10}$$

that is

$$\mathbf{X}(E_{\mathbf{p}}) = -\mathbf{p}\exp(i\sigma_1)C(1,\eta')\ . \tag{B11}$$

Appendix C: Partial Wave decomposed Coulomb Green's Function

We now continue by analyzing the Coulomb Green's function $(\mathbf{r}_1|G_{\rm C}|\mathbf{r}_2)$. It is useful to express the Green's function in its partial wave expanded form

$$(\mathbf{r}_1|G_{\rm C}(E)|\mathbf{r}_2) = \sum_{l=0}^{\infty}(2l+1)G_{\rm C}^{(l)}(E;r_1,r_2)P_l(\hat{\mathbf{r}}_1\cdot\hat{\mathbf{r}}_2)\ . \tag{C1}$$

The form of $G_{\rm C}^{(l)}$ is derived by expanding the Coulomb wavefunctions in Eq. (3), using spherical harmonics. In the first step we use the orthogonality of the harmonics and in the second step the addition theorem is used:

$$\begin{aligned}(\mathbf{r}_1|G_{\rm C}(E)|\mathbf{r}_2) &= \sum_{l_1m_1}\sum_{l_2m_2}\int\frac{{\rm d}^3p}{(2\pi)^3}\frac{(4\pi)^2}{(2l_1+1)(2l_2+1)}\frac{\phi_{l_1}(\eta,\rho_1)\phi^*_{l_2}(\eta,\rho_2)}{E-\frac{\mathbf{p}^2}{2m_{\rm R}}}\\ &\quad\times Y_{l_1m_1}(\theta_1,\varphi_1)Y^*_{l_1m_1}(\theta_p,\varphi_p)Y_{l_2m_2}(\theta_p,\varphi_p)Y^*_{l_2m_2}(\theta_2,\varphi_2)\\ &= \sum_{lm}\int\frac{{\rm d}^3p}{(2\pi)^3}\frac{4\pi}{(2l+1)^2}\frac{\phi_l(\eta,\rho_1)\phi^*_l(\eta,\rho_2)}{E-\frac{\mathbf{p}^2}{2m_{\rm R}}}\times Y_{lm}(\theta_1,\varphi_1)Y^*_{lm}(\theta_2,\varphi_2)\\ &= \sum_{l}\frac{P_l(\hat{\mathbf{r}}_1\cdot\hat{\mathbf{r}}_2)}{2l+1}\int\frac{{\rm d}^3p}{(2\pi)^3}\frac{\phi_l(\eta,\rho_1)\phi^*_l(\eta,\rho_2)}{E-\frac{\mathbf{p}^2}{2m_{\rm R}}}\ .\end{aligned} \tag{C2}$$

Thus, the Green's function for a specific partial wave is given by

$$(2l+1)G_{\rm C}^{(l)}(E;r_1,r_2) = \frac{1}{2l+1}\int\frac{{\rm d}^3p}{(2\pi)^3}\frac{\phi_l(\eta,\rho_1)\phi^*_l(\eta,\rho_2)}{E-\frac{\mathbf{p}^2}{2m_{\rm R}}}\ . \tag{C3}$$

We are now in a position to simplify the integral

$$I_1(0,\mathbf{r}) = \int\frac{{\rm d}^3k}{(2\pi)^3}\mathbf{k}\langle\mathbf{k}|G_{\rm C}(E)|\mathbf{r}\rangle\ . \tag{C4}$$

Note that it is defined by a mixed matrix element where the Coulomb Green's function is evaluated between a bra in k-space and a ket in r-space. Comparing to the S-wave equivalent

$$\begin{aligned}I_0(0,\mathbf{r}) &= \int\frac{{\rm d}^3k}{(2\pi)^3}\langle\mathbf{k}|G_{\rm C}(E)|\mathbf{r}\rangle\\ &= (0|G_{\rm C}(E)|\mathbf{r})\ ,\end{aligned} \tag{C5}$$

we expect that I_1 behaves as an r-space object. Using Eq. (B7) and doing a partial wave expansion of $\psi^*_{\mathbf{p}}(\mathbf{r})$, we have

$$\begin{aligned} I_1(0,\mathbf{r}) &= \int \frac{\mathrm{d}^3k\mathrm{d}^3p}{(2\pi)^6}\mathbf{k}\,\psi_{\mathbf{p}}(\mathbf{k})\frac{\psi^*_{\mathbf{p}}(\mathbf{r})}{E-\frac{\mathbf{p}^2}{2m_{\mathrm{R}}}} \\ &= \sum_l \int \frac{p^2\mathrm{d}p}{(2\pi)^3} i \lim_{\rho'\to 0}\Big(\frac{\phi_1(\eta,\rho')}{\rho'}\Big)\frac{\phi^*_l(\eta,\rho)}{E-\frac{\mathbf{p}^2}{2m_{\mathrm{R}}}}\int \mathrm{d}\Omega_{\mathbf{p}} P_l(\cos\theta) \\ &= i\frac{\hat{\mathbf{r}}}{3}\lim_{\mathbf{r}'\to 0}\Big[\frac{1}{r'}\int\frac{\mathrm{d}^3p}{(2\pi)^3}\frac{\phi_1(\eta,\rho')\phi^*_1(\eta,\rho)}{E-\frac{\mathbf{p}^2}{2m_{\mathrm{R}}}}\Big]\,. \end{aligned} \tag{C6}$$

Finally, using Eq. (C3) we find that

$$\begin{aligned} I_1(0,\mathbf{r}) &= \int\frac{\mathrm{d}^3k}{(2\pi)^3}\mathbf{k}\langle\mathbf{k}|G_{\mathrm{C}}(E)|\mathbf{r}) \\ &= 3i\hat{\mathbf{r}}p\lim_{\mathbf{r}'\to 0}\Big(\frac{G^{(1)}_{\mathrm{C}}(E;r',r)}{\rho'}\Big)\,. \end{aligned} \tag{C7}$$

This form is useful since the partial wave projected Green's function can be written in a closed functional form. Eq. (C7) can be further simplified using Eq. (A15).

---

[1] E. G. Adelberger, A. B. Balantekin, D. Bemmerer, C. A. Bertulani, J. -W. Chen, H. Costantini, M. Couder and R. Cyburt *et al.*, Rev. Mod. Phys. **83** (2011) 195.

[2] S. R. Beane, P. F. Bedaque, W. C. Haxton, D. R. Phillips and M. J. Savage, In *Shifman, M. (ed.): At the frontier of particle physics, vol. 1* 133-269.

[3] P. F. Bedaque and U. van Kolck, Ann. Rev. Nucl. Part. Sci. **52** (2002) 339.

[4] E. Epelbaum, H. W. Hammer and U. -G. Meißner, Rev. Mod. Phys. **81** (2009) 1773.

[5] C. A. Bertulani, H.-W. Hammer and U. Van Kolck, Nucl. Phys. A **712**, 37 (2002).

[6] P. F. Bedaque, H.-W. Hammer and U. van Kolck, Phys. Lett. B **569** (2003) 159.

[7] J. Rotureau and U. van Kolck, Few Body Syst. **54** (2013) 725.

[8] C. Ji, C. .Elster and D. R. Phillips, arXiv:1405.2394 [nucl-th].

[9] D. L. Canham and H. -W. Hammer, Eur. Phys. J. A **37** (2008) 367.

[10] P. Hagen, H. -W. Hammer and L. Platter, Eur. Phys. J. A **49** (2013) 118.

[11] G. Rupak and R. Higa, Phys. Rev. Lett. **106** (2011) 222501.

[12] L. Fernando, R. Higa and G. Rupak, Eur. Phys. J. A **48** (2012) 24.

[13] X. Zhang, K. M. Nollett and D. R. Phillips, Phys. Rev. C **89** (2014) 024613.

[14] H. -W. Hammer and D. R. Phillips, Nucl. Phys. A **865** (2011) 17.

[15] G. Rupak, L. Fernando and A. Vaghani, Phys. Rev. C **86** (2012) 044608.

[16] B. Acharya and D. R. Phillips, Nucl. Phys. A **913** (2013) 103.

[17] B. Acharya, C. Ji and D. R. Phillips, Phys. Lett. B **723** (2013) 196.

[18] G. Hagen, P. Hagen, H. -W. Hammer and L. Platter, Phys. Rev. Lett. **111** (2013) 13, 132501.

[19] X. Kong and F. Ravndal, Phys. Lett. B **450** (1999) 320.

[20] X. Kong and F. Ravndal, Nucl. Phys. A **665** (2000) 137.

[21] S.-I. Ando, J. W. Shin, C. H. Hyun and S. W. Hong, Phys. Rev. C **76** (2007) 064001.

[22] T. Barford and M. C. Birse, Phys. Rev. C **67** (2003) 064006.

[23] S.-I. Ando and M. C. Birse, Phys. Rev. C **78** (2008) 024004.

[24] R. Higa, H. -W. Hammer and U. van Kolck, Nucl. Phys. A **809** (2008) 171.

[25] E. Ryberg, C. Forssén, H.-W. Hammer and L. Platter, Phys. Rev. C **89** (2014) 014325.

[26] X. Zhang, K. M. Nollett and D. R. Phillips, Phys. Rev. C **89** (2014) 051602.

[27] K. M. Nollett and R. B. Wiringa, Phys. Rev. C **83** (2011) 041001.

[28] P. Navrátil, R. Roth and S. Quaglioni, Phys. Lett. B **704** (2011) 379.

[29] G. Tabacaru, A. Azhari, J. Brinkley, V. Burjan, F. Carstoiu, C. Fu, C. A. Gagliardi and V. Kroha *et al.*, Phys. Rev. C **73** (2006) 025808.

[30] M. Abramowitz and I.A. Stegun, *Handbook of Mathematical Functions*, Dover Publications, New York (1964).

[31] D. Bollé and F. Gesztesy, Phys. Rev. A **30** (1984) 1279.

[32] S. König, D. Lee and H.-W. Hammer, J. Phys. G **40** (2013) 045106.

[33] D.R. Tilley, C.M. Cheves, J.L. Godwin, G.M. Hale, H.M. Hofmann, J.H. Kelley, C.G. Sheu and H.R. Weller, Nucl. Phys. A **708** (2002) 3.

[34] S. Pastore, S. C. Pieper, R. Schiavilla and R. B. Wiringa, Phys. Rev. C **87** (2013) 035503.

[35] A. Ong, J. C. Berengut and V. V. Flambaum, Phys. Rev. C **82** (2010) 014320.

[36] B. W. Filippone, A. J. Elwyn, C. N. Davids and D. D. Koetke, Phys. Rev. Lett. **50** (1983) 412.

[37] F. Hammache, G. Bogaert, P. Aguer, C. Angulo, S. Barhoumi, L. Brillard, J. F. Chemin and G. Claverie *et al.*, Phys. Rev. Lett. **80** (1998) 928.

[38] F. Hammache, G. Bogaert, P. Aguer, C. Angulo, S. Barhoumi, L. Brillard, J. F. Chemin and G. Claverie *et al.*, Phys. Rev. Lett. **86** (2001) 3985.

[39] M. Hass *et al.* [ISOLDE Collaboration], Phys. Lett. B **462** (1999) 237.

[40] F. Strieder *et al.*, Nucl. Phys. A **696** (2001) 219.

[41] L. T. Baby *et al.* [ISOLDE Collaboration], Phys. Rev. Lett. **90** (2003) 022501 [Erratum-ibid. **92** (2004) 029901].

[42] A. R. Junghans, E. C. Mohrmann, K. A. Snover, T. D. Steiger, E. G. Adelberger, J. M. Casandjian, H. E. Swanson and L. Buchmann *et al.*, Phys. Rev. C **68** (2003) 065803.

[43] A. R. Junghans, K. A. Snover, E. C. Mohrmann, E. G. Adelberger and L. Buchmann, Phys. Rev. C **81**, 012801 (2010).

[44] G. Papadimitriou, A. T. Kruppa, N. Michel *et al.*, Phys. Rev. C **84** (2011) 051304.